

Contents

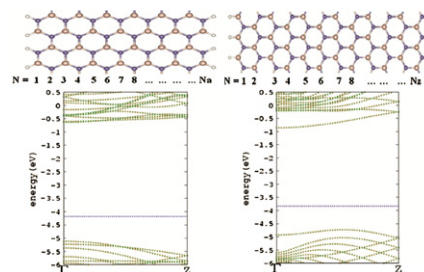
EDITOR'S CHOICE

181–186

First-principle studies of electronic structure and C-doping effect in boron nitride nanoribbon

A.J. Du, Sean C. Smith, G.Q. Lu

Geometry structure and two typical band structures for H-terminated boron nitride nanoribbon (BNNR) with armchair and zigzag shaped edge.



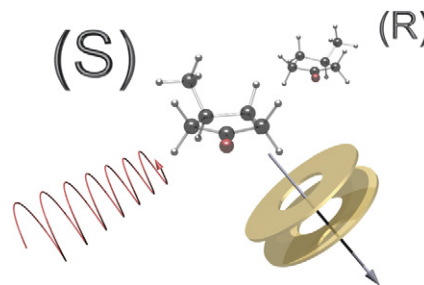
GASEOUS MOLECULES

187–191

Investigation of CD effects in the multi photon ionisation of R-(+)-3-methylcyclopentanone

Alexander Bornschlegl, Christoph Logé, Ulrich Boesl

Resonance enhanced multi photon ionisation (MPI) allows to combine electronic CD spectroscopy and time-of-flight mass spectrometry by using circularly polarised laser light. Different MPI-excitation schemes have been investigated. New CD effects have been observed comparing one- and two-colour experiments.

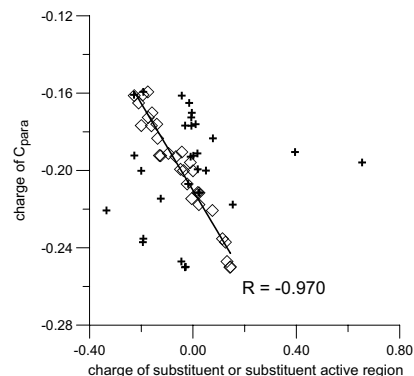


192–196

Substituent active region – a gate for communication of substituent charge with the rest of a molecule: Monosubstituted benzenes

N. Sadlej-Sosnowska

The highly disordered relationship between potential at C_{para} in the benzene ring and charge of the substituent turns into good linear one when charge of the substituent active region is considered instead.

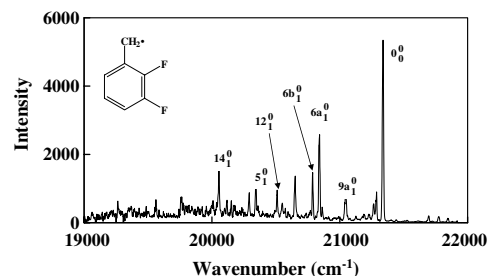


197–201

Vibronic emission spectra of jet-cooled 2,3-difluorobenzyl radical in a corona excited supersonic expansion

Gi Woo Lee, Hyeon Geun Ahn, Tae Kyu Kim, Sang Kuk Lee

Observation of vibronic emission spectra of jet-cooled 2,3-difluorobenzyl radical in a corona excited supersonic expansion.

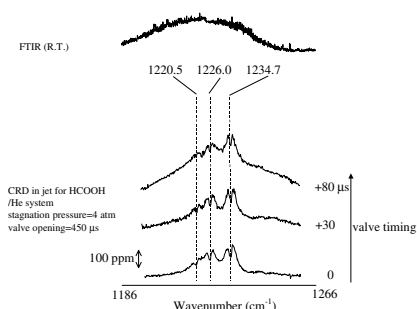


202–207

Jet-cooled infrared spectra of the formic acid dimer by cavity ring-down spectroscopy: Observation of the C–O stretching region and vibrational analysis of the Fermi-triad system

Fumiyuki Ito

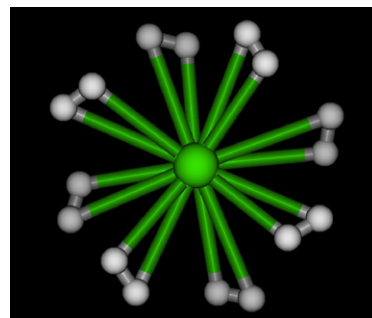
A jet-cooled infrared spectrum of formic acid dimer in the C–O stretching region. The low rotational temperature attained in the jet enabled us to observe three vibrational bands which are not resolved at room temperature (upper trace).



208–214

Electrostatics driven interaction of dihydrogen with s-block metal cations: Theoretical prediction of stable MH₁₆ complex

K.R.S. Chandrakumar, Swapan K. Ghosh

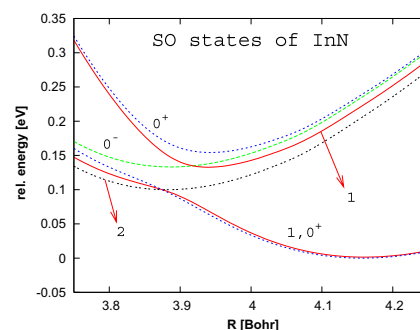
Theoretical prediction of the formation of complexes between s-block metal ions and dihydrogen molecules, MH₁₆, is reported. The number of hydrogen molecules attached to the metal cation is the highest ever known in the literature.

215–220

Improved theoretical calculations of InN in its X³Σ[−] ground state and in the first ³Π excited state

Lukáš Demovič, Ivan Černušák, Giannoula Theodorakopoulos, Ioannis D. Petsalakis, Miroslav Urban

Spectroscopic constants of the ground and the first excited state of InN are calculated using CCSD(T), CASPT2, CASPT2/RASSI-SO, and MRCI methods.



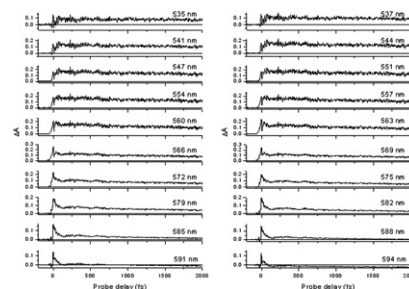
CONDENSED PHASES

221–226

Real-time vibrational amplitude change in the ground and excited states of a quinoid thiophene induced by few-cycle pulses

Zhuan Wang, Takayoshi Kobayashi

Vibrational amplitude change after 6.7 fs pulse excitation taking place in a quinoid thiophene was observed within two picoseconds.

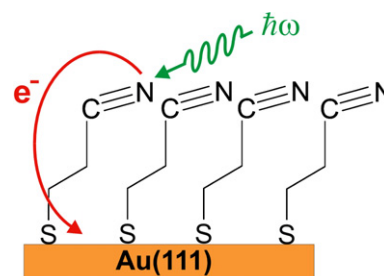


227–231

Charge transfer dynamics in self-assembled monomolecular films

S. Neppi, U. Bauer, D. Menzel, P. Feulner, A. Shaporenko, M. Zharnikov, P. Kao, D.L. Allara

Femtosecond electron transfer dynamics in highly ordered self-assembled monolayers of nitrile-terminated alkanethiols is investigated using resonant Auger spectroscopy.

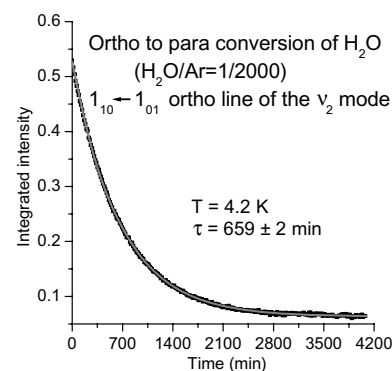


232–235

Nuclear spin conversion of water diluted in solid argon at 4.2 K: Environment and atmospheric impurities effects

L. Abouaf-Marguin, A.-M. Vasserot, C. Pardanaud, X. Michaut

We show that the NSC of H₂O diluted in solid argon is due to an enhancement of intramolecular spin-rotation coupling by solid argon environment.

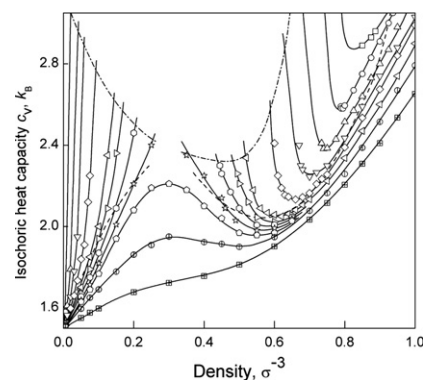


236–240

The isochoric heat capacity of a metastable Lennard-Jones fluid

V.G. Baidakov, S.P. Protsenko, Z.R. Kozlova

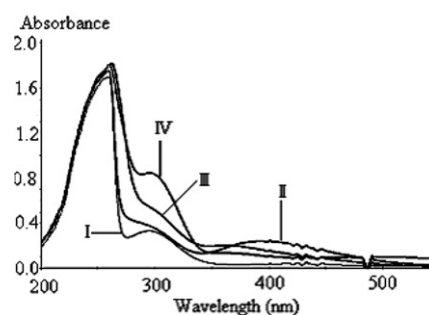
The isochoric heat capacity of the fluid passes through a minimum and continues to increase when approaching the spinodal (dashed-dotted lines).



241–246**The concurrence of photoreduction and bromination of 1,4-benzoquinone in aqueous solution**

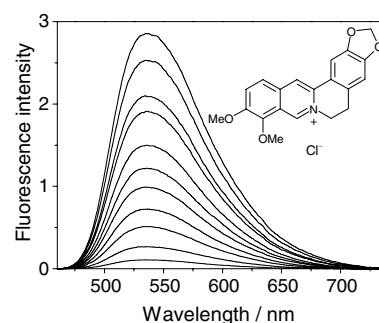
Nan Li, James R. Green, Jichang Wang

Absorption spectra showing the light-mediated 1,4-benzoquinone–bromine reaction, which leads to the production of bromated 1,4-hydroquinones.

**247–251****Effect of ion pairing on the fluorescence of berberine, a natural isoquinoline alkaloid**

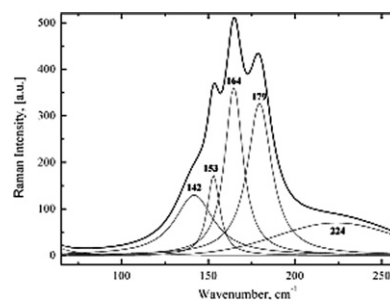
Mónika Megyesi, László Biczók

Association with chloride or perchlorate anions leads to considerable change in the fluorescence properties of berberine, a cationic isoquinoline alkaloid.

**NANOSTRUCTURES AND MATERIALS****252–256****Radiation damage and Raman vibrational modes of single-walled carbon nanotubes**

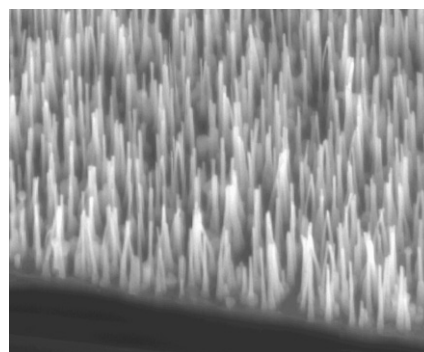
U. Ritter, P. Scharff, O.P. Dmytrenko, N.P. Kulish, Yu.I. Prylutskyy, N.M. Belyi, V.A. Gubanov, L.A. Komarova, S.V. Lizunova, V.V. Shlapatskaya, H. Bernas

Raman scattering for the radial and tangential vibrational modes of single-walled carbon nanotubes (CNT) with different absorption doses of high-energy electron irradiation were explored. New vibrational modes both for the armchair and zigzag CNT appear and a substantial change in the intensities and broadening are observed for the high-frequency Raman bands with high absorption doses.

**257–262****Effect of incident fluence on the growth of ZnO nanorods by pulsed excimer laser deposition**

Ye Sun, Rachel P. Doherty, James L. Warren, Michael N.R. Ashfold

The role of incident fluence upon the morphology of ZnO nanorod arrays grown by pulsed UV laser deposition is demonstrated and rationalised.

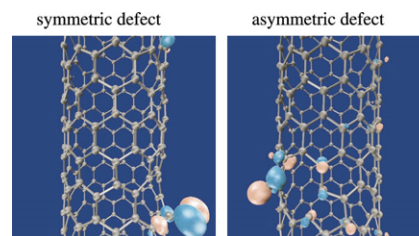


263–267

Energetics and electronic structures of carbon nanotubes with adatom–vacancy defects

Susumu Okada

Isosurfaces of the squared wave function for the lowest unoccupied states of the (11, 0) nanotubes with the adatom–vacancy defects of which configuration are symmetric and asymmetric to the tube axis. In the asymmetric defect, the states exhibit extended character compared with the symmetric one.

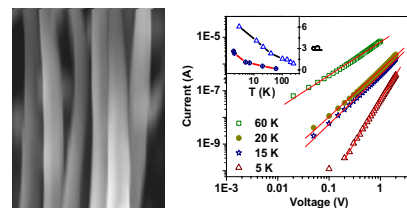


268–273

Enhancement of electron–electron interactions in chemically synthesized polymer nanowires

Atikur Rahman, Milan K. Sanyal, Rupali Gangopadhyay, Amitabha De

Electronic transport properties of conducting polymer nanowires synthesized by chemical and electrochemical method show power-law current–voltage characteristics at low temperature. Large value of the power-law exponent indicates enhancement of electron–electron interactions in chemically synthesized nanowires.

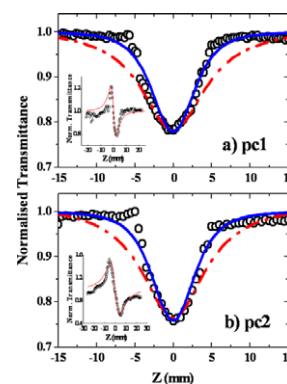


274–278

Femtosecond and nanosecond nonlinear optical properties of alkyl phthalocyanines studied using Z-scan technique

R. Sai Santosh Kumar, S. Venugopal Rao, L. Giribabu, D. Narayana Rao

We report strong nonlinear absorption properties of alkyl phthalocyanines studied using Z-scan technique with 800 nm femtosecond and 532 nm nanosecond pulses.

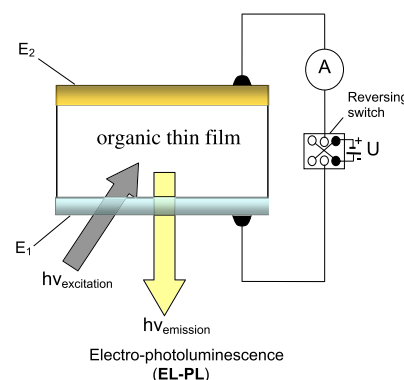


279–283

Electro-photoluminescence in organics

J. Kalinowski, M. Cocchi, D. Virgili, V. Fattori, J.A.G. Williams

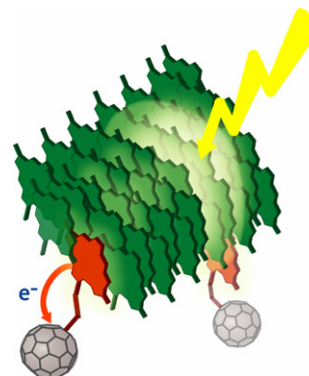
A successful observation of the steady-state electro-photoluminescence (EL-PL) is reported in thin, exciplex emitting, organic solid films. It shows up as either an enhancement or quenching of the PL output, dependent on the electric field applied and light excitation intensity.



284–288**An artificial supramolecular photosynthetic unit**

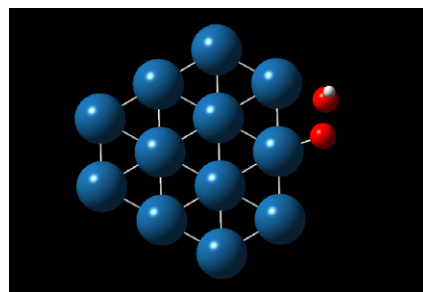
Martin Katterle, Valentyn I. Prokhorenko, Alfred R. Holzwarth, Aldo Jesorka

A self-assembled antenna mimics the supramolecular light-harvesting structure and an embedded dyad acts both as energy acceptor and charge transfer dyad.

**289–294****OOH dissociation on Pt clusters**

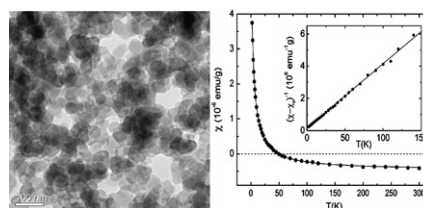
Yuguang Ma, Perla B. Balbuena

Activation barriers for O–O dissociation on the cluster edges are reduced in one order of magnitude respect to those on the center of the cluster.

**295–299****Magnetic properties of dense carbon nanospheres prepared by chemical vapor deposition**

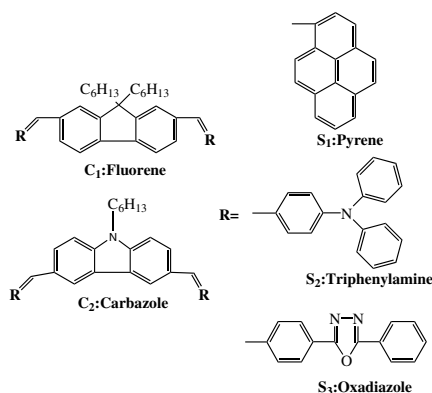
José M. Calderón-Moreno, Amílcar Labarta, Xavier Batlle, Trinitat Pradell, Daniel Crespo, Vu Thien Binh

Paramagnetic carbon nanospheres: The stable paramagnetic spins are located inside the solid carbon, at interfaces between graphitic-amorphous clusters.

**300–304****A two-photon absorption study of fluorene and carbazole derivatives. The role of the central core and the solvent polarity**

I. Ftilis, M. Fakis, I. Polyzos, V. Giannetas, P. Persephonis, P. Vellis, J. Mikroyannidis

The role of the central core and the solvent polarity on two-photon absorption of fluorene and carbazole derivatives is studied.

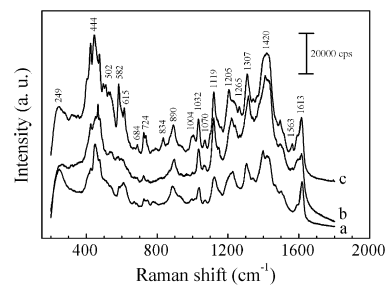


305–309

Surface-enhanced Raman scattering of methylene blue adsorbed on cap-shaped silver nanoparticles

Gui-Na Xiao, Shi-Qing Man

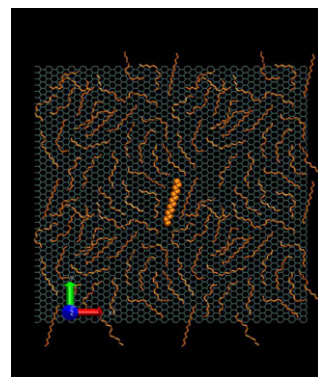
SERS spectra of methylene blue adsorbed on cap-shaped silver nanoparticles.



310–315

Surface diffusion of *n*-alkanes: Mechanism and anomalous behavior

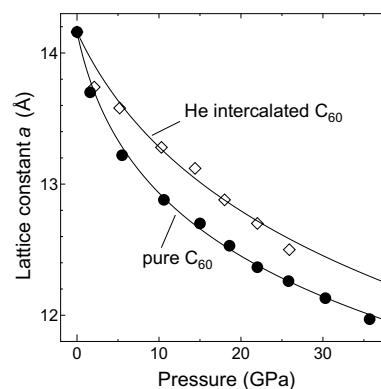
Jae Hyun Park, N.R. Aluru

Graphical depiction of *n*-tetradecane molecules on a graphite surface when the surface is fully covered.

316–319

He intercalated C₆₀ solid under high pressure

S. Kawasaki, T. Hara, A. Iwata

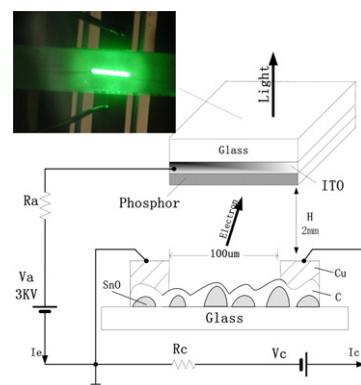
This is the first study to precisely investigate the structural property of the He intercalated C₆₀ under high pressure in a few tens GPa range.

320–323

Electron emission from carbon film on island-like tin oxide layer

Dan Zhu, Dejie Li, Jian Wang

A new type of electron emitter composed of carbon film on island-like tin oxide layer is realized with 1% efficiency.



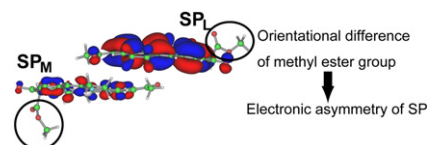
BIOMOLECULES

324–329

Theoretical analysis of the electronic asymmetry of the special pair in the photosynthetic reaction center: Effect of structural asymmetry and protein environment

Hideki Yamasaki, Haruki Nakamura, Yu Takano

The effect of the protein environment and the structural difference on the electronic structure of the special pair and the special pair cation radical in the photosynthetic reaction center were studied with density functional theory using polarizable continuum model and point charge model.

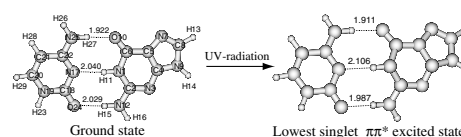


330–334

Evidence of structural non-planarity in excited state: New findings provided by vibrational analysis of the guanine–cytosine base pair

M.K. Shukla, G.M. Kuramshina, Jerzy Leszczynski

Vibrational frequency analysis for the Watson–Crick guanine–cytosine (GC) base pair in the ground and lowest single $\pi\pi^*$ excited state was performed based on the reference geometry optimized at the HF/6-311G(d,p) and CIS/6-311G(d,p) levels, respectively. It was found that different NH and CH stretching vibrations can be used for the qualitative prediction of excited state geometrical non-planarity and the localization of electronic excitations in the base pair complexes.

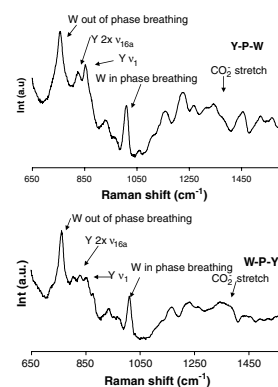


335–339

Competitive binding effects on surface-enhanced Raman scattering of peptide molecules

Leo Seballos, Nicole Richards, Daniel J. Stevens, Mira Patel, Laura Kapitzky, Scott Lokey, Glenn Millhauser, Jin Z. Zhang

Various tyrosine (Y), proline (P) and tryptophan (W) containing peptides were studied to understand molecular binding on a SERS substrate.



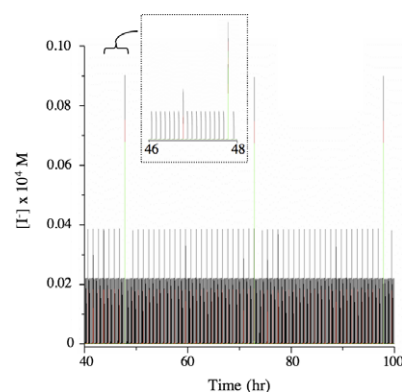
NEW EXPERIMENTAL OR THEORETICAL METHODS

340–344

A true chemical clock: Serially coupled chlorite–iodide oscillators

David A. Long, Leah Chodroff, Tim M. O'Neal, Sheryl Hemkin

A theoretical chemical clock results from a model of coupled reactors that oscillate with frequencies of minutes, hours, and days.

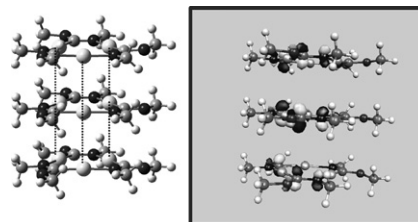


345–351

Theoretical study on electronic spectra and auerophilic attraction in $[\text{Au}_3(\text{MeN}=\text{COMe})_3]_n$ ($n = 1\text{--}4$) complexes

Fernando Mendizabal, Benjamín Aguilera, Claudio Olea-Azar

The auerophilic attraction and the spectroscopic properties of $[\text{Au}_3(\text{MeN}=\text{COMe})_3]_n$ ($n = 1\text{--}4$) were studied. All complexes showed MMCT and MLCT transitions interrelated with the gold–gold intermolecular distanced.

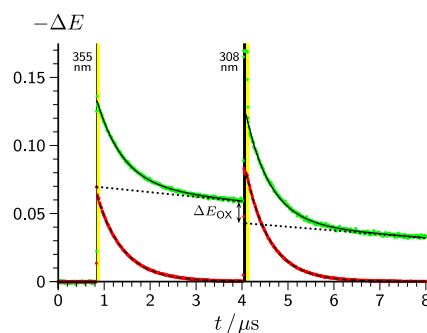


352–357

The photoreduction of $[\text{Ru}(\text{bpy})_3]^{3+}$ investigated by two-pulse two-colour laser-flash photolysis

Martin Goez, Daniel von Ramin-Marro

A direct investigation of this reaction is impossible because of chemical instability, but two-laser experiments do the trick.

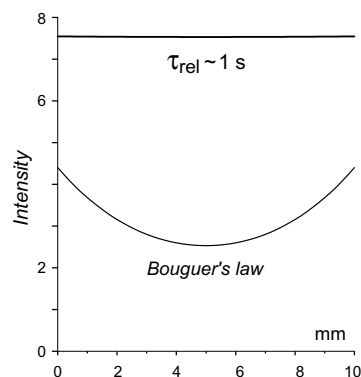


358–363

Peculiarities of light propagation through the media of molecules with long-lived photoexcited states

Marina V. Olenchuk, Yuri M. Barabash, Leonid N. Christophorov, Valeriy N. Kharkyanen

Light intensity distribution in a two-side illuminated sample 10 mm length as compared with that given by Bouguer's law.

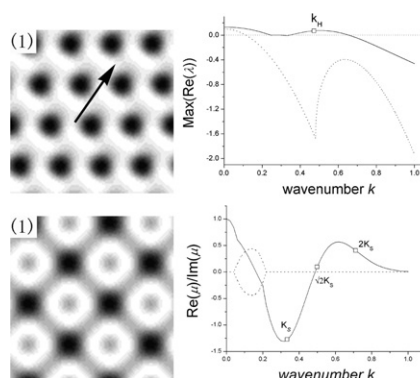


364–367

Traveling and standing patterns induced by delay feedback in uniform oscillatory reaction–diffusion system

Hai Xiang Hu, Qian Shu Li, Se Li

We investigate influence of delay feedback on pattern formation in reaction–diffusion system. Delay feedback unusually induces two instabilities.

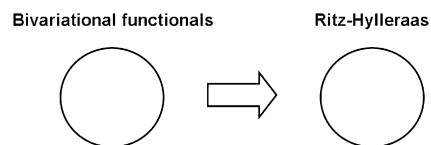


368–369

Bivariational functionals and the Ritz-optimized second-order Hylleraas functional

Valerio Magnasco, Michele Battezzati

It is shown that the ordinary form of the Ritz-optimized Hylleraas functional is a particular case of the general determinantal equation derived in the case of bivariational functionals.

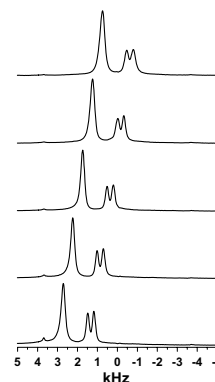


370–374

A broad-banded z-rotation windowed phase-modulated Lee–Goldburg pulse sequence for ^1H spectroscopy in solid-state NMR

Michal Leskes, P.K. Madhu, Shimon Vega

The design and experimental implementation of an effective z-rotation wPMLG sequence for ^1H spectroscopy in solid-state NMR is demonstrated with a scale factor independent of radio-frequency imperfections.

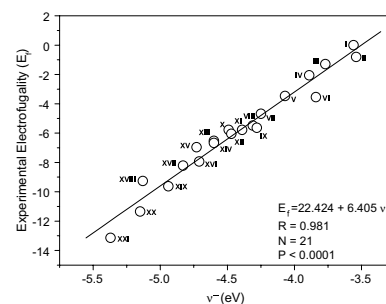


375–378

Electrofugality index for benzhydryl derivatives

Paola R. Campodónico, Claudio Pérez, Margarita Aliaga, Marcela Gazitúa, Renato Contreras

The regional electron-donating power at the nucleophilic end of a molecule assesses well its electrofugality pattern.

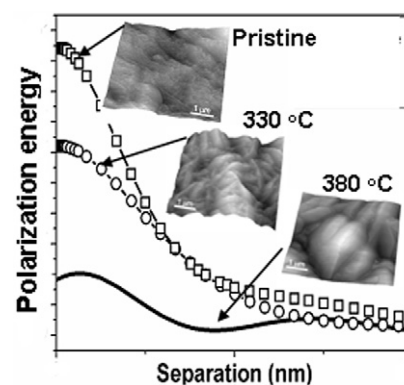


379–383

Line tension at high contact angle wetting: Contribution to interfacial energy at long distances ($\gg 100$ Å) from the triple line contour

O. Teschke, E.F. de Souza

Line tension effect on the water/air interfacial energy induced by the texture of PTFE substrates where air bubbles are anchored.



384–387
On the largest eigenvalue of the distance matrix of a connected graph
Bo Zhou, Nenad Trinajstić

Some properties of the largest eigenvalue λ_1 of the distance matrix of a connected graph, such as the upper and lower bounds for λ_1 , are reported. The relationship between λ_1 and the first Zagreb index and the Wiener index is given. Additionally, the Nordhaus–Gaddum-type result for λ_1 is also presented.

$$\sqrt{\frac{\sum_{i=1}^n D_i^2}{n}} \leq \lambda_1(G) \leq \max_{1 \leq i \leq n} \sum_{j=1}^n D_{ij} \sqrt{\frac{D_j}{D_i}}$$

Author Index of Volume 388

The Publisher encourages the submission of articles in electronic form thus saving time and avoiding rekeying errors. Please refer to the online version of the Guide for Authors at <http://www.elsevier.com/locate/cplett>



Full text of this journal is available, on-line from **ScienceDirect**. Visit **www.sciencedirect.com** for more information.